Geophys. J. Int. (2006) **165,** 73–86 doi: 10.1111/j.1365-246X.2006.02877.x

Geomagnetic secular variation of Bransfield Strait (Western Antarctica) from analysis of marine crossover data

M. Catalán,[1] L. M. Agudo[1] and Alfonso Muñoz[2]

[1] *Real Instituto y Observatorio de la Armada, San Fernando* 11000, *Cádiz, Spain. E-mail: mcatalan@roa.es*
[2] *Univ. Complutense de Madrid, Facultad de Ciencias Geológicas, Dpto. de Geodinámica,* 28040 *Madrid, Spain*

Accepted 2005 November 16. Received 2005 October 24; in original form 2004 December 16

SUMMARY

Tracking the secular variation of the geomagnetic field in the past is severely limited in some cases by factors relating to the remoteness of the sites. This is maximal in the Antarctic where the remote location and severe climate lead to logistic limitations that make it difficult to keep a continuous record of magnetic field variations. From the magnetic information available from historical marine expeditions, it is possible to infer this time-varying component from the comparison of readings at crossovers. This study focuses on this technique, discusses the impact of the different error sources and proposes a simple mathematical procedure to infer average secular variation rates. The result is validated by comparing it with local data from the Arctowski and Livingston magnetic observatories, sited in the area. Additionally, using a high-quality data set from a local area in the neighbourhood of Deception Island, we have detected a systematic distribution in its secular variation. This dichotomy has been interpreted in terms of a volcano-magnetic signal. This fact and the nature of its principal mechanisms are analysed and discussed.

Key words: Antarctica, geomagnetic secular variation, magnetic anomalies, volcanic activity.

1 INTRODUCTION

The Earth's geomagnetic field is a dynamic concept which covers periods ranging from a fraction of a second to millions of years. High frequency domain is related to what are known as external contributions mainly caused by the influence of the sun.

The so-called 'main field' generated in the Earth's outer core justifies more than 90 per cent of our magnetic field. The main field varies slowly in time and can be described by mathematical models, such as the International Geomagnetic Reference Field (IGRF), which was originally updated every 5 yr. This situation has been modified and improved by the availability of unprecedented high-quality data from the latest satellite missions, making a higher rate of newer version releases possible [International Association of Geomagnetism and Aeronomy (IAGA), Division V, Working Group 8, 2003].

Traditionally, one of the most important tasks undertaken by magnetic observatories was to determine the annual rate of change or secular variation (*SV*) of the main field. This *SV* differs from place to place and varies in time.

As it is so remote, the Antarctic continent has always suffered from a shortage of information, particularly that derived from magnetic observatories. In an area larger than 11 million km^2, only 25 observatories have been in operation south of 60° S since 1960. Their distribution has been both irregular and discontinuous over time. Potential errors in the modelling of regional magnetic fields and their secular variation are common due to this lack of information.

As the magnetic field of the Earth varies over time, the extremely good perspective available nowadays through magnetic satellite missions cannot be projected to the past or corrected by the use of future satellite missions or by increasing the density of secular variation sites. This is why the use of historical data from geophysical cruises is a possibility worth considering.

2 GEOLOGICAL SETTING

The area of interest for this study lies between the Antarctic Peninsula and the South Shetland archipelago (Fig. 1). This area (Bransfield Strait) is considered as a backarc basin related to the South Shetland Islands volcanic arc. It consists of a 500 km long extensional structure with a well-marked NE–SW orientation developed during the Upper Cenozoic, ceasing abruptly to the southwest. Hero fracture extension marks this limit, while the conclusion is more gradual to the northeast (Southern Scotia plate) (González-Casado *et al.* 2000, Figs 1 and 2).

Parra *et al.* (1984) modelled aeromagnetic data and suggested an age of 1.8 Ma for the start of the basin opening at an average full rate velocity of 0.9 cm yr^{-1}. González-Ferrán (1991) suggests, from aeromagnetic data interpretation, an average full spreading rate of 0.25–0.75 cm yr^{-1} for the past 2 Ma. However, there is no strong

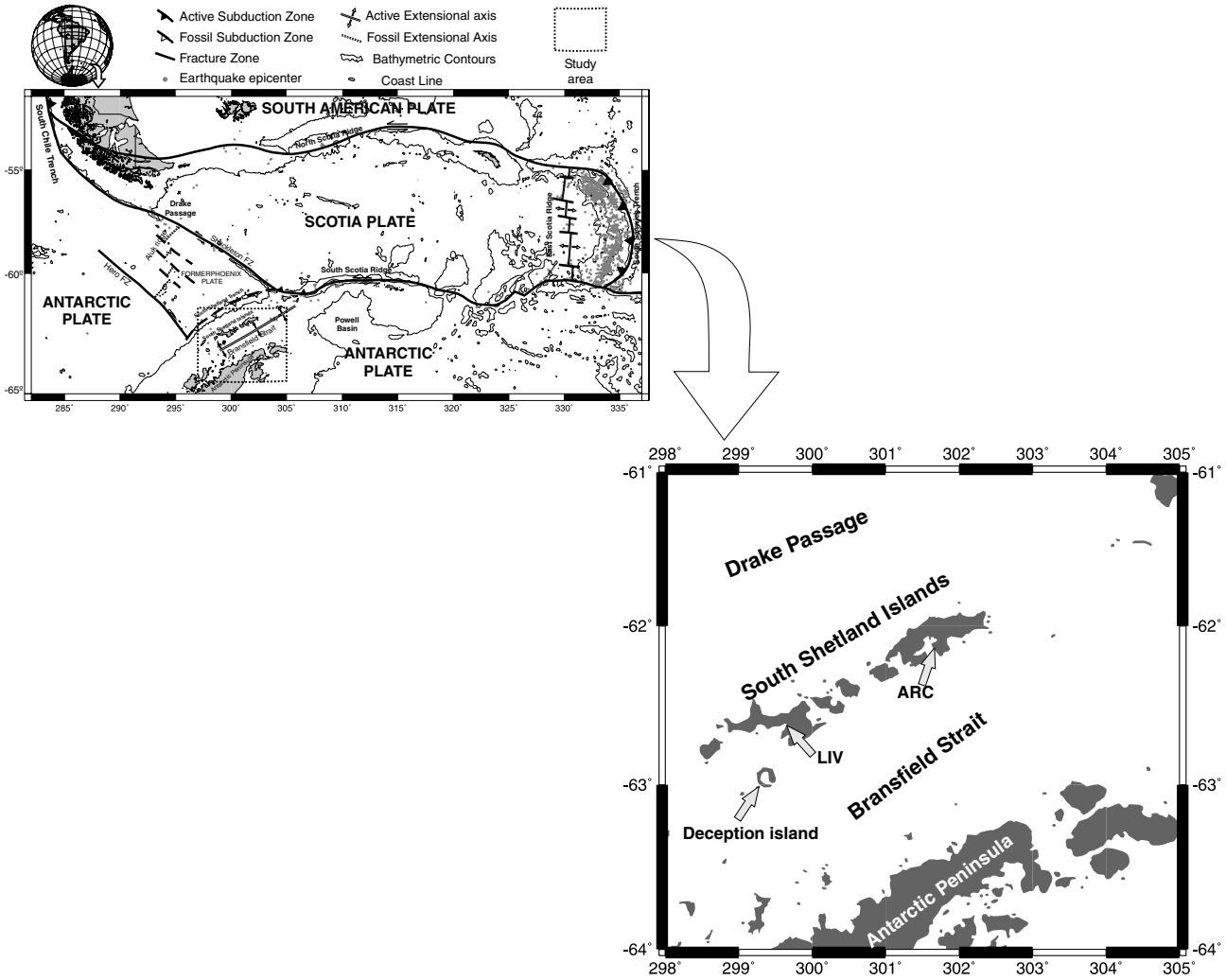

Figure 1. Regional geotectonic framework of the area and location of the South Shetland Islands. Main geological features are included as well as Arctowski and Livingston magnetic observatory locations.

evidence for normal seafloor spreading within the basin due to its youth, which makes the magnetic patterns diffuse (Lawver *et al.* 1996). Nevertheless, its magmatic activity is well established, with subaerial as well as submarine volcanism episodes, so it will be of use in the second part of this study.

Swath bathymetry records show the linear trend of these volcanic features, roughly aligned along the basin (Canals *et al.* 1994; Gràcia *et al.* 1996). Quaternary volcanism is recorded at Deception Island, as well as at several other places in the South Shetland Islands.

Deception Island (DI) forms the emerged part of a young active shield volcano (less than 1 Myr). It lies in the south-western Bransfield Strait. This area has been the subject of different geophysical research projects, especially into seismic reflection (Acosta *et al.* 1992; Barker & Austin 1994, 1998; Prieto *et al.* 1998), magnetics (Roach 1978), structural studies (Gràcia *et al.* 1996, 1997; González-Casado *et al.* 1999; Baraldo & Rinaldi 2000), seismotectonics (Pelayo & Wiens 1989; Ibáñez *et al.* 2000), seismic refraction (Grad *et al.* 1992; Barker *et al.* 2003) and airborne gravimetry (Garrett 1990). Recent stratigraphic work has been carried out at DI (Baraldo & Rinaldi 2000) providing bulk magnetic susceptibilities analyses.

Finally, in relation to temporal geomagnetic monitoring in Bransfield Strait, we must point out that the Arctowski observatory (ARC) was established in 1978, at the Polish Base of the same name on King George Island (Fig. 1). This observatory ceased operations in December 1995 (Polish Academy of Sciences 1998). Livingston Island observatory (LIV) started operations in December 1996 and took over the ARC's study of secular variations in the area (Torta *et al.* 1999, 2001) (Fig. 1).

3 DATA COMPILATION

The use of marine proton magnetometers allowed precise magnetic data to be made available without questioning the stability of the platform (i.e. fluxgate sensor limitation). This information has existed on a worldwide scale, particularly in the Antarctic, since the 1960s. In this study, we have compiled marine magnetic data from the Geophysical Data System (GEODAS) (Metzger & Campagnoli 2003). A total of 20 cruises covered the period 1961–2002, as well as other geophysical campaigns carried out by the Royal Observatory of the Spanish Navy during several austral summers: 1989–90, 1990–91, December 1999 and January–February 2002.

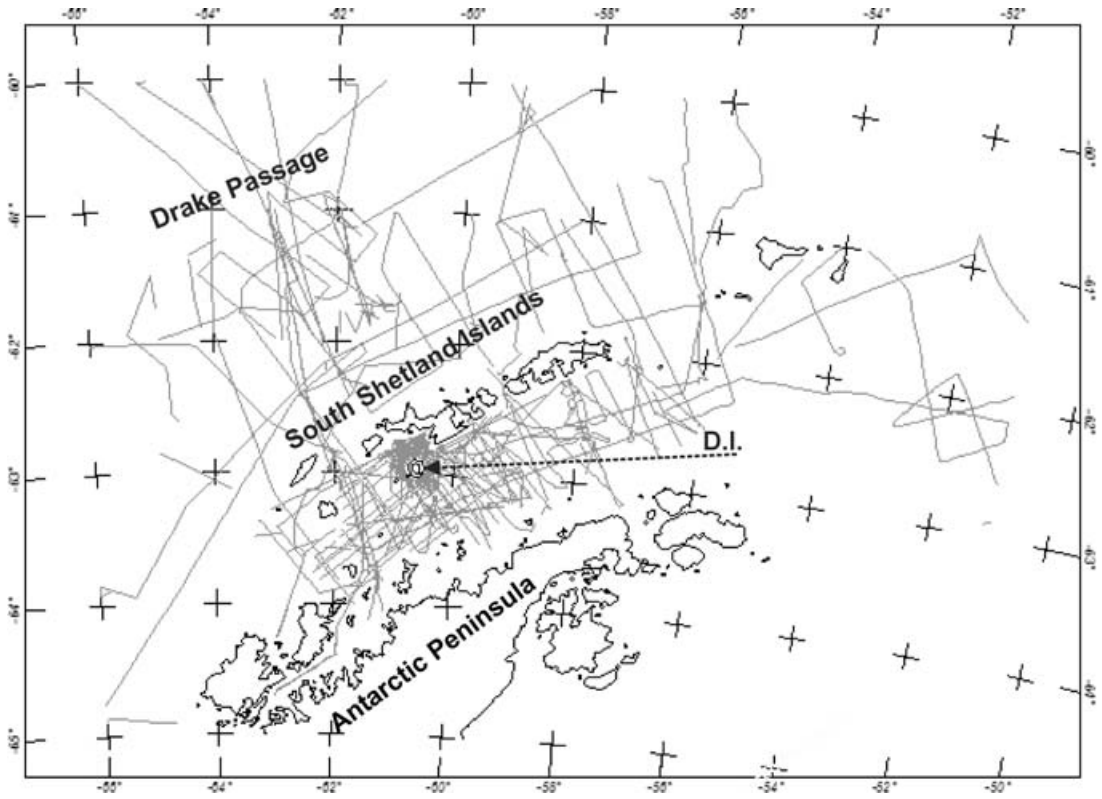

Figure 2. Marine track line coverage in the area. D.I.: Deception Island.

The spatial coverage of data for the area (Fig. 2) is dense, especially in the immediate neighbourhood of DI. The temporal coverage may be appreciated in Fig. 3. It is not strictly uniform; it shows some gaps, mainly in the mid-1980s. We will see that although marine cruises do not offer a continuous time recording, we should still be sensitive to the effect since, in the case of secular variation, we are interested in a long-term signal.

Crossover analyses are used to estimate the quality of a geophysical survey as well as to provide an effective technique for improving the internal coherency of geophysical data grids (Wessel & Watts 1988; Thakur *et al.* 1999). Since, in general terms, the local magnetic anomaly is time-invariant, if we examine the crossover difference between two tracks, the residue will contain information related to time-dependent geomagnetic field components *SV* and external field contributions.

A 702-crossover data set was obtained. We arranged the different crossovers into homogeneous groups according to the survey epoch involved, i.e. crossovers derived from cruises which took place in 1961.33 and 2002.17 were arranged separately from those derived by crossing 1971.9 and 1999.33 cruises.

In order to reduce the influence of external fields, only periods with moderate or low magnetic activity were used, inferring it from the range of the *kp* indices ($kp \leq 3$). For each period of time, we derived the mean and standard deviation values for the different crossover residuals obtained throughout. The latter will contribute to average any short-term time-dependent error source.

We could consider our average *SV* data set as representative for the whole area, and in particular for the DI surroundings. The last (the tie point data set was not really derived from any particular location) is not really relevant as, generally speaking, secular variation has a global morphology. Thus, the difference in secular changes between sites some tens of kilometres apart are usually negligible. We can check from the map (Fig. 4) that the expected variation in *SV* values for the area of interest is in the range of 2 nT yr^{-1}. We have represented our results in Fig. 5(a).

4 ERROR ESTIMATES

A magnetic survey generally suffers from different sources of error:

(a) An incomplete cancellation of external contributions.

(b) An indirect effect produced by a possible lack of precision in the position of the ship. This fact, considering the local magnetic field gradient, could generate differences in crossover readings near the coast where the spatial gradient is maximized.

(c) Instrumental errors.

4.1 External contributions

External field contributions are usually extracted by using reference stations (e.g. magnetic observatories). None of our records were corrected for this effect, except the last two cruises, DECVOL and GEODEC. This is due to several reasons: the remote situation of the study area, the logistic and technical difficulties in having an operative magnetic reference station, the lack of magnetic observatories and/or the difficulty of finding available observatory data.

This feature establishes two groups in relation to the precision of the surveys. The first one merges the whole data set, except the DECVOL (Dec 1999) and GEODEC (Jan–Feb 2002) cruises, which used LIV data to extract external field contributions.

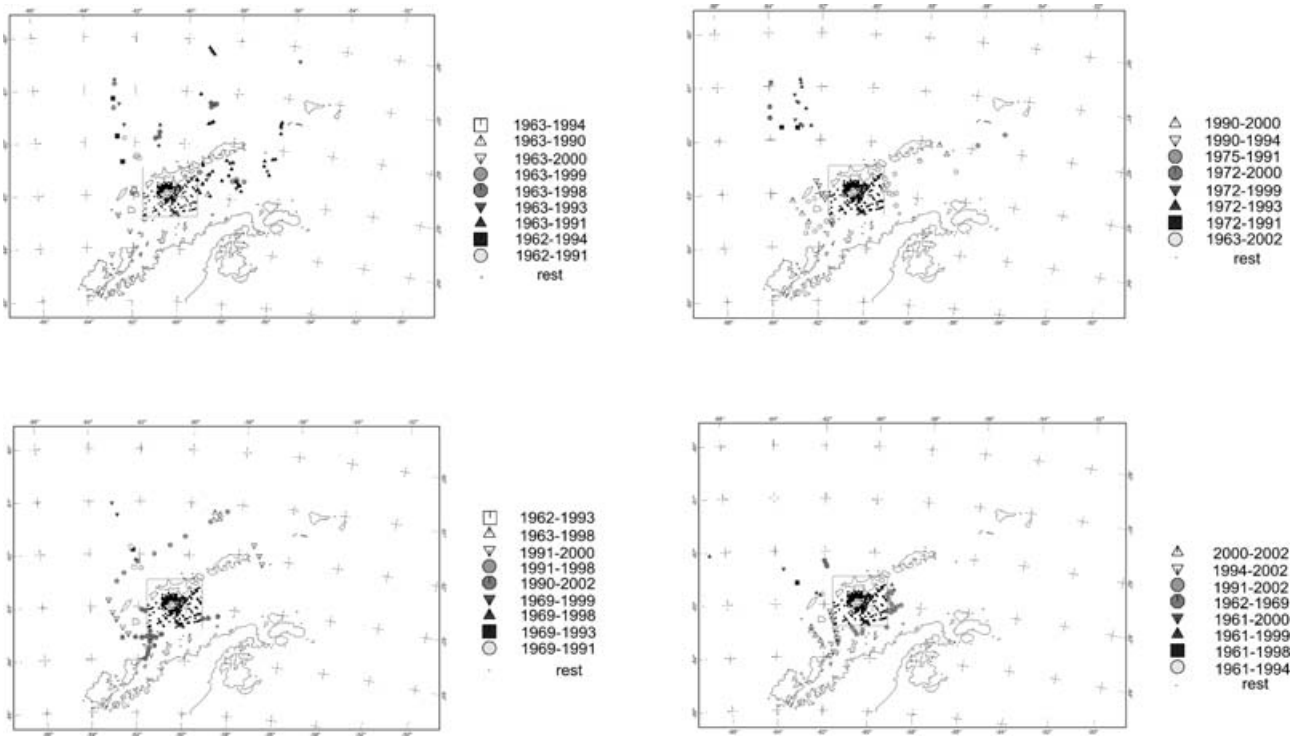

Figure 3. Spatial and temporal distribution of the crossovers. As nearly 70 per cent of all the crossover data set is included in the immediate neighbourhood of Deception Island, for the sake of clarity we have not used the polygon code but a rectangle plot to mark the location of every crossover inside it (black dot points) and have indicated this feature with a label called 'rest' in the colour range symbol legend.

We consider external field contributions to be the error source which could potentially have the greatest impact. In fact, when we compare two cruises at a tie point, to infer an isolated *SV* measure, this error contribution could reach tens of nT. In particular, we should emphasize that, according to the Livingston observatory's magnetic records, the external magnetic field shows an average amplitude of about 50 nT.

4.2 Ship's position

This second error source contributes to making our data set inhomogeneous mainly because it covers a wide temporal range. It would, *a priori*, show the effect of historical technical improvements, especially in precision positioning since this has advanced considerably. We have been able to verify, from early cruise header information, that their position was astronomical and also based on dead reckoning.

Celestial navigation achieved a practical accuracy of 2 or 3 km, which is enough for oceanic navigation purposes but *a priori* makes scientific study difficult. Dead reckoning complemented the previous technique, however nothing can be said concerning its accuracy because it depended on the precision of the knowledge of other factors such as wind, current, helmsman error, etc. Even if the navigator maintained this position-fixing technique for a long time without celestial observation confirmations, this method could lead to kilometric errors in position.

Although not reflected in the cruise header information, radar as well as visual bearings may have been used when sailing near the coast in the first surveys, even the very earliest ones. This would have significantly improved the precision of their position when the cruises sailed near the coast, obtaining an error on position measured in hundreds of metres.

Positioning was later based on satellite Doppler techniques and, finally, in the early 90s, it came to be based on the Global Positioning System (GPS). The former satellite-based system provided an accuracy of roughly 200 m and the latter shows an error on position of just under 100 m. However, on 1st May 2000, the 'Selective Availability' code was turned off, allowing all users (military and civilian) to enjoy almost the same level of access, with a precision of less than 20 m.

As can be appreciated in Fig. 2, the tie point distribution almost always falls near the coast, which makes it quite plausible that navigation could have been based on visual bearings or radar in earlier times. Therefore, they may have been accurate to hundreds of metres.

Taking into account that the analytical signal grid gives quite a good representation of the magnetic gradient distribution for the whole marine area of interest, we derived that the highest absolute value of the horizontal magnetic gradient in the whole area remains less than 0.007 nT m^{-1}.

For the earliest cruises that must have used radar or visual bearings, 200 m would be a reasonable position error impact and could be considered as a conservative threshold for those cruises that used satellite-based techniques. Considering the average magnetic gradient cited (0.007 nT m^{-1}) and the threshold proposed for position error, it seems difficult to expect this error contribution to have an impact worth taking into account in the magnetic readings.

Nevertheless, we cannot ignore the fact that slightly less than 70 per cent of the whole crossover data set lies in the area surrounding Deception Island (Fig. 3). This area presents higher gradients due to its volcanic character. A detailed analytical signal grid for the

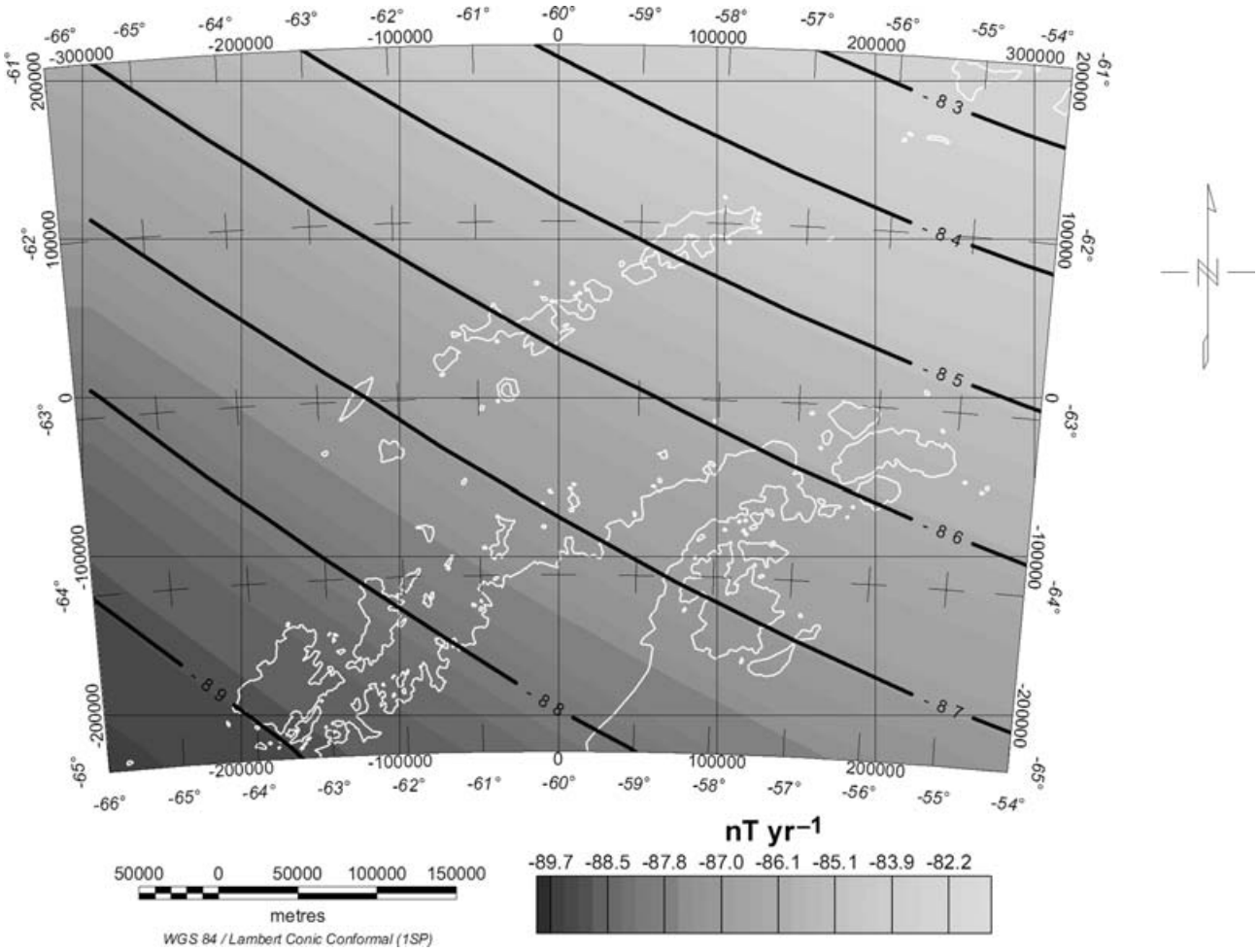

Figure 4. Secular variation (*SV*) of the area of study. We have observed that the *SV* shows values from −83 to −89 nT yr^{-1}.

Deception Island area shows an average gradient of 0.08 nT m^{-1}, while the maximum value of 0.19 nT m^{-1} may be considered as an upper limit that was not exceeded by 92 per cent of the values. The latter means that some values greater than 0.19 nT m^{-1} were found but are not representative from a statistical point of view.

Considering, once again, that 200 m may reasonably represent position error, this could justify an expected upper limit error contribution for uncertainty in navigation of about 40 nT (in the worst case).

4.3 Instrumental errors

In relation to instrumental errors, we must point out that our considerable experience with these types of instruments (proton precision magnetometers) allows us to affirm that this contribution would be less than a few units of nT. Therefore, its influence on the *SV* calculus would not only be less than 1 nT yr^{-1} but would also be averaged out because we merge different instruments.

To sum up, we have two main error sources: lack of precision in the position of the ship and an incomplete cancellation of external field contributions. Their impact on the error budget is difficult to assess *a priori*. It depends on whether the cruises were (or were not) corrected by ground reference stations (most of them were not) and the uncertainties regarding location vary according to the technique used.

Nevertheless, a value of 40 nT may be considered as the upper limit for positioning errors, with a value of 50 nT for the impact of external field contributions.

4.4 Secular variation values

We get the secular variation values by using finite differences. Additionally, we have derived *SV* values for fixed periods of time (i.e.: 1961.33–1994.25, 1961.33–1999.33) by grouping the geophysical cruises that were carried out during the same periods of time and, finally, we have derived averaged *SV* values. Following these criteria, we have obtained a set of 42 groups.

We wish to highlight that the earliest cruises were often not really systematic geophysical surveys but navigations where the proton magnetometer was towed. In this regard, they do not provide more than one or two tie points when crossed with other cruises.

These values have been analysed in detail one by one (i.e. the quality of the crossing) and consider the 1962.95–1991.17 cruise as a reference which provides, after 66 crossings, an *SV* estimation equal to -99.9 ± 4 nT yr^{-1}. This value was used as a reference and caused us to disregard certain cruises whose *SV* estimation,

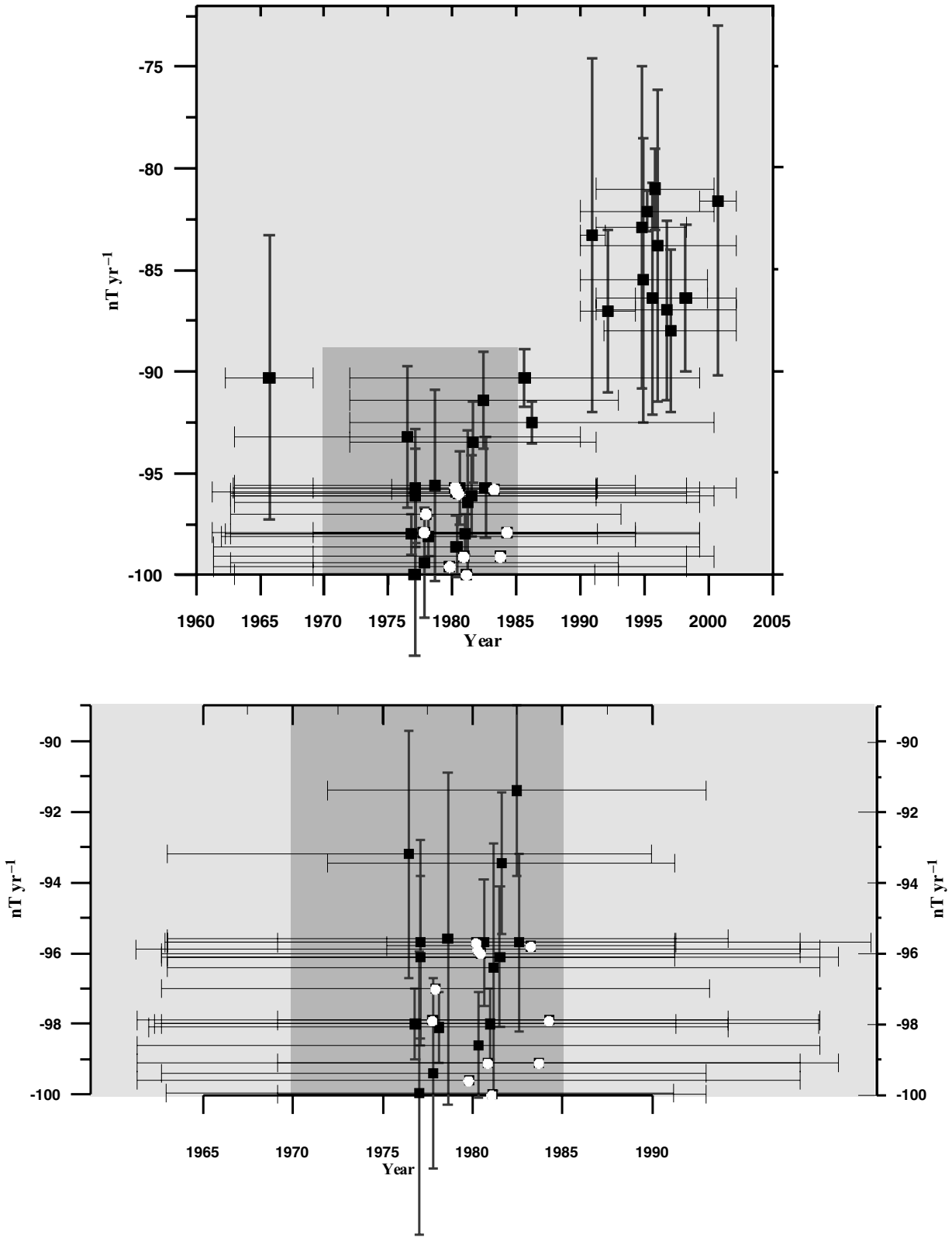

Figure 5. (a) The apparent average of the *SV* rate is displayed with solid black squares overprinting a black horizontal bar which indicates the time span it averages. Thick grey vertical bars indicate the standard deviation (error bars).White solid circles represents those *SV* estimations based on less than three crossovers. (See text for comments) (b) As most of the information concentrates the middle of its time span around the 1980s, this subplot contains the same information as in Fig. 5(a) but shows 1965–1990 in greater detail. (See text for comments).

based on one or two readings, clearly differed from the latter (i.e. -109 nT yr^{-1}).

All these *SV* estimations, based only on one or two samples, were included in Figs 5(a) and (b) but without standard deviation and displayed as solid white circles.

The 42 *SV* values have an average character and the impact of the different error sources will be reduced varyingly according to the duration of the time span. This is particularly true when we derive the average *SV* of the earliest periods, when positioning always lacked precision. In the case of other, later cruises (in the 1980s, 1990s or 2000s), the denominator always remains greater than 10, contributing to reduce this possible error contribution by at least one order of magnitude. The situation is similar concerning external field contributions.

Additionally, the crossover data set used to derive average *SV* values for fixed periods of time (i.e. 1991.33–1994.25) involves different track cruises with no systematisation concerning the time of acquisition. Hourly and short-time variations will be averaged out, at least partially, over such a time span.

Although we concede that this reasoning is quite speculative (and it cannot be otherwise, considering the information we have available), the standard deviation obtained for every time period (Fig. 5) shows the internal coherency of the *SV* series and serves to confirm the limited impact of the error sources cited previously.

Generally speaking, Fig. 5(a) shows a systematisation where the greatest variability concerns comparisons between the most recent cruises, showing the attenuating effect induced by the time span upon different error sources.

This feature (time span) reduces the different error impacts by at least one order of magnitude when the earliest cruises are compared with the most modern ones (i.e. 1961.33–1999.33), as opposed to comparisons between cruises separated by smaller periods of time, even if they used better positioning techniques (i.e. 1989.95–1994.25).

The South Atlantic and nearby areas present isoporic foci. Although the variation rates of the different geomagnetic elements are not constant, they reach maximum values (nearly 100 nT yr^{-1} for total field). This fact will simplify our study, minimizing the impact (in relative terms) of the different error sources.

5 DISCUSSION OF RESULTS

5.1 Secular variation

In Figs 5(a) and (b), the values of the average *SV* for different periods of time from 1961.33 to 2002.17 are presented together with their standard deviation. In spite of their average character, they show consistency and we can infer some consequences.

Two main clusters in the temporal *SV* evolution may be discerned from the image (Fig. 5a), showing a continuous increase in its amplitudes with time. Amplitudes of around -85 nT yr^{-1} for the later years become slightly smaller than -95 nT yr^{-1} when we include the earliest periods (1961, 1962 and 1963) in the calculations.

Generally speaking, the absolute *SV* values obtained for periods that include the 1990s show greater amplitudes (about -85 nT yr^{-1}) than previously inferred (nearly -95 nT yr^{-1}).

Finally, we must highlight that the group which merges the most recent cruises (1999–2002 cruises) shows the greatest *SV* amplitudes (nearly -80 nT yr^{-1}). As this time span is not only short but is also the most recent one, this *SV* value could be used to infer the most representative *SV* value (at the moment) for the area.

Table 1. Date of occurrence of jerk events.

Date of occurrence of the Jerk	(yr)	References
t_{JR1}	1972.1	(Alexandrescu *et al.* 1996; De Michelis *et al.* 1998)
t_{JR2}	1981.5	(Alexandrescu *et al.* 1996)
t_{JR3}	1990.1	(De Michelis *et al.* 2000)
t_{JR4}	1999.0	

Recent studies have revealed sudden changes, which occur from time to time, in the *SV* trend. These features have been called 'geomagnetic jerks' (De Michelis *et al.* 1998, 2000; Mandea *et al.* 2000; Bloxham *et al.* 2002). During the 20th century several events were detected; the last three, which occurred in the second half of the century, in 1969, 1978 and 1990, were worldwide in character (Bloxham *et al.* 2002). A recent study published by Mandea *et al.* (2000) suggests, from magnetic measurements taken at some European observatories, the possibility of a new geomagnetic jerk around 1999. Their occurrence and duration seem to be geographically dependent and they tend to take place over a 2-yr interval or less.

We could express every averaged *SV* residual in the following general mathematical form:

$$\begin{aligned}\Delta(t_i, t_j) = {} & SV_1^*(t_{JR1} - t_i) + SV_2^*(t_{JR2} - t_{JR1}) \\ & + SV_3^*(t_{JR3} - t_{JR2}) + SV_4^*(t_{JR5} - t_{JR4}) \\ & + SV_5^*(t_j - t_{JR5}),\end{aligned} \tag{1}$$

where $\Delta(t_i, t_j)$ expresses the residual obtained by comparing two crossover readings at epochs $\boldsymbol{t_i}$ and $\boldsymbol{t_j}$. SV_k expresses the average secular variation corresponding to the period of time, which is considered between brackets. The symbol t_{JRk} expresses the date of occurrence of the jerk event, which, as has already been noted, is geographically dependent.

Following Alexandrescu *et al.* (1996) and De Michelis *et al.* (1998), we have selected 1972.1 as the date of occurrence for the 1969 event. In the same regard, and according to Alexandrescu *et al.* (1996) and De Michelis *et al.* (2000), we have selected, respectively, 1981.5 and 1990.1 as the dates for the 1978 and 1991 events in the area.

As far as we know, there is no available study of the 1999 event, except the already-cited study by Mandea *et al.* (2000), which could serve to mark its date of occurrence. Given these conditions, we have arbitrarily selected 1999.0 as the date of occurrence for our calculus.

We have a data set of 42 crossover residuals which span the 1961.33–2002.17 time period. In matrix notation, eq. (1) may be written in the following manner:

$$[\Delta] = [SV][\Delta t] \tag{2}$$

and *SV* are (42 × 1) and (5 × 1) column vectors, respectively, while Δt is a (42 × 5) matrix. The matrix Δt is the design matrix which relates crossover residuals and the different *SV* rates between jerk events. Strictly speaking, we must point out that *SV* varies all the time and it does not behave as a step-like function since it is inferred from eq. (1) or its matrix expression (eq. 2).

These equations express a linear relationship. In order to be coherent with this simplification, we prefer to work with smaller residuals. For this reason, we prefer to arrange eq. (2) in the following form:

$$[\Delta] = [SV_o + sv][\Delta t] \tag{3}$$

Table 2. *A priori SV* values derived after the different *SV* Coefficients (from 1962 to 2003) provided by the DGRF models for the studied area (see text for details).

$SV1_O$ (nT yr^{-1})	$SV2_O$ (nT yr^{-1})	$SV3_O$ (nT yr^{-1})	$SV4_O$ (nT yr^{-1})	$SV5_O$ (nT yr^{-1})
−108	−102	−93	−88	−83.7

Table 3. *SV* values obtained after applying the least-square iterative process on the whole data set.

$SV1$ (nT yr^{-1})	$SV2$ (nT yr^{-1})	$SV3$ (nT yr^{-1})	$SV4$ (nT yr^{-1})	$SV5$ (nT yr^{-1})
−106.0	−100.0	−91.2	−87.0	−83.6

$$[\Delta] - [SV_o][\Delta t] = [sv][\Delta t] \tag{4}$$

$$[\zeta] = [sv][\Delta t], \tag{5}$$

where ζ is a (42 × 5) matrix which shows, through the magnitude of its components, its disagreement with the *a priori SV* values (SV_O).

The different SV_O values (see Table 2) were derived from the different *SV* values (from 1962 to 2003) provided by the DGRF models at a location situated in the middle of the rectangle that holds almost 70 per cent of the crossover data set (Latitude −63°, Longitude −61°) and were validated every first of January.

This one sample/year DRGF series was averaged out during the following periods of time: 1961.3–1972.1, 1972.1–1981.5, 1981.5–1990.1, 1990.1–1999.0 and 1999.0–2002.2.

Nevertheless, we must point out that for the first period (1961.3–1972.1) the DGRF provides a mean value equal to −80.8 nT yr^{-1} that is clearly unrealistic according to our *SV* data, which suggest smaller values. In fact, when we resolve our solution for this first period, using the suggested DGRF mean value, it always provides values below −100 nT yr^{-1}, in fact nearly −108 nT yr^{-1}.

We believe that the DGRF value for the period 1961.3–1970 is inaccurate. For this reason, and according to our previous results, we have selected −108 nT yr^{-1} as the first SV_O value.

To solve eq. (5) we have used an iterative (conjugate-gradient-like) method (Paige & Saunders 1982) which solves the least-squares solution for the $\boldsymbol{sv}$ matrix that minimizes $\|\zeta - sv\Delta t\|$. Finally, the following values for the $\boldsymbol{SV}$ matrix were obtained with a relative residual equal to 0.23 (Table 3), with the relative residual materialized by the following mathematical expression:

$$\frac{\|\zeta - sv\Delta t\|}{\|\zeta\|}. \tag{6}$$

In order to check our results, we have obtained the different *SV* values that correspond to the period 1978–2003 by using the Arctowski observatory annual geomagnetic means for the period 1978–1995 and accordingly using the Livingston observatory annual geomagnetic means for the period 1998–2003. They are plotted as solid black circles in Fig. 6.

These *SV* values were interpolated at one sample/year rate in order to avoid the gap that goes from the end of ARC operations to the onset of LIV. Later, we obtained *SV* mean values for the periods of time that are represented by our *SV* results: 1979.0–1981.5; 1981.5–1990.1; 1990.1–1999.0 and 1999.0–2002.3. These *SV* mean values are included as grey segments in Fig. 6. The *SV* values obtained in this study are displayed with solid black lines (Table 3).

We can see a reasonable agreement between observed *SV* values and those inferred from the marine crossover data set. In particular, the monotonic increase seems to be confirmed.

As the use of *SV* averages obtained from very few samples would be questionable, we have checked a solution obtained using only averages derived from four or more crossovers (see Table 4). These *SV* mean values are included as dashed black segments in Fig. 6.

We wanted to emphasize the 1979.0–1981.5 period, for which the ARC observatory proposes −97.8 nT yr^{-1} while our algorithm (using the whole *SV* series) produces −100 nT yr^{-1}. Although this difference is not so great when compared with the *SV* series obtained after using only selected *SV* values, we must highlight the fact that our solution provides the value that best fits over a wider period of time (1962–2002) and particularly the period 1972.1–1981.5.

As a result, we consider that our proposed *SV* probably gives a better representation of the average *SV* in this area than the other (derived from the ARC observatory), which considers only three values. This would be supported by the fact that the other three solutions agree quite closely with the expected values from the observatories' yearly averages. Additionally, the first yearly averages from ARC seem to show smaller values (Fig. 6). If this trend were maintained throughout the previous decade, the final average value would have been significantly close to our value.

5.2 A special local secular variation feature in the Deception Island neighbourhood

As has been previously noted, the DECVOL and GEODEC cruises were the most precise of all because we used DGPS techniques to position the ship and the marine records were corrected by using nearby reference stations: the LIV station and another located on Deception Island.

In Fig. 7 we have represented the *SV* values inferred from the crossover comparison between the two cruises mentioned above. Although they seem to be about −75 nT yr^{-1}, we noticed a dichotomy in which the smallest *SV* amplitudes (−81.1 ± 8.6 nT yr^{-1}) were located on the northern side of DI (Fig. 7: inside black dashed polyline) while the greater *SV* amplitudes (−60.8 ± 6 nT yr^{-1}) were situated in the southern part (Fig. 7: outside black dashed polyline).

The scalar magnetic field map of the area, as well as the Bouguer anomaly map (Muñoz *et al.* 2005), shows a high gradient in the north of DI with a NE–SW trend. Seismic models study the local upper crustal structure (Grad *et al.* 1992), showing an inclined boundary in this area with a velocity of about 6.1 km s^{-1}. Velocities of 6.3–6.7 km s^{-1} are observed in the south of this high gradient anomaly. Magnetic models detect a clear susceptibility contrast between average north and south susceptibility (0.07 I.S.) (Muñoz *et al.* 2005). This linear feature has been interpreted as a separation of two different upper crust domains: the first one, located north of DI, would be compatible with a standard continental crystalline basement versus a more altered one in the south.

The smaller *SV* amplitude data group shows remarkable correlation with the northern upper crust domain, while the greater

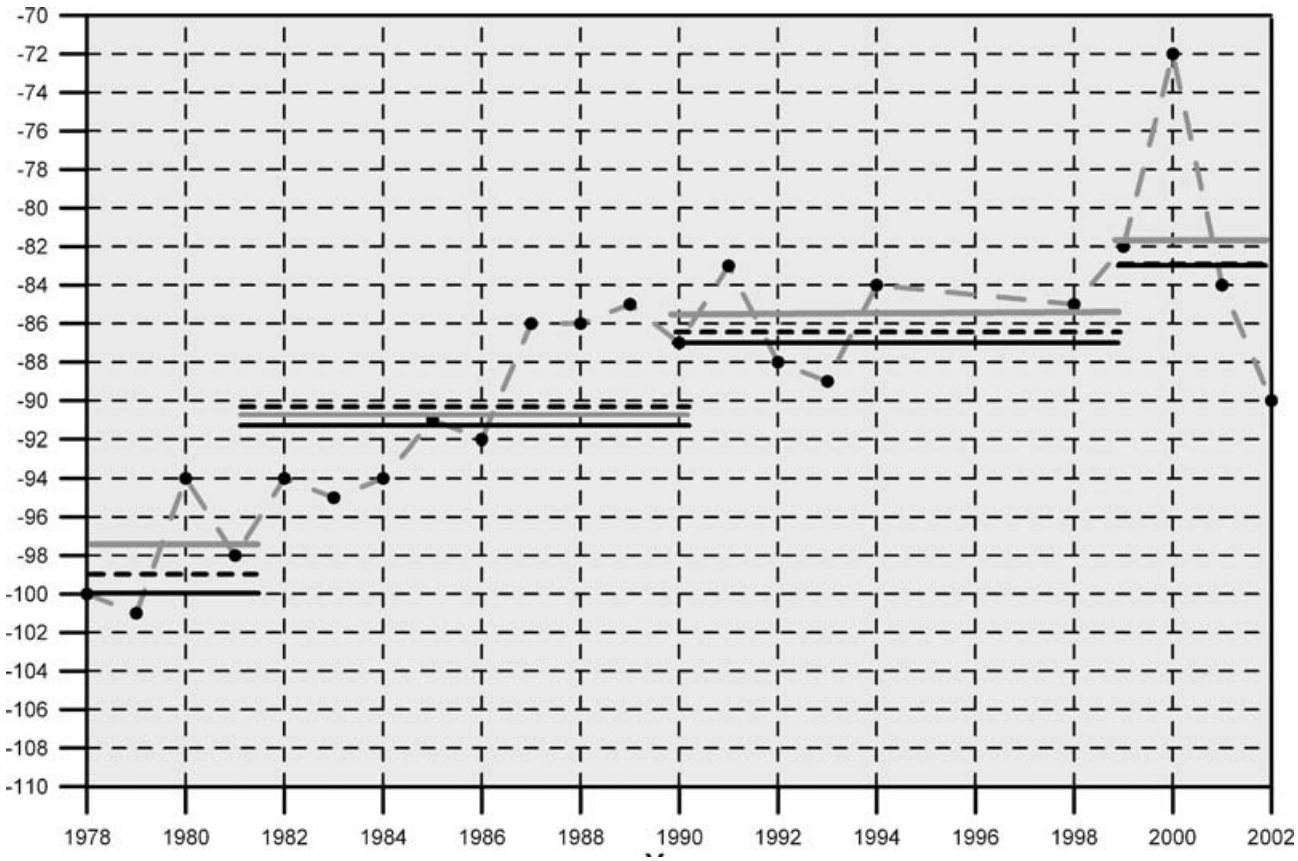

Figure 6. Comparison of *SV* values obtained throughout this paper with those from the Arctowski (1978–1995) and Livingston observatories (1998–2002). Solid black circles (overprinting the grey dashed line) represent the 'Arctowski & Livingston' average *SV* yearly series. Solid black segments show the average *SV* values obtained in this study using the whole *SV* average series, while black dashed segments show the average *SV* values obtained using only selected *SV* averages (derived from more than 4 crossovers). Grey segments represent the average *SV* values obtained from the 'Arctowski & Livingston' average yearly series.

SV group seems to be distributed throughout the southern side (Fig. 7).

In general, the scalar magnetic measurement reflects the influence of three sources: internal fields, external fields and crustal contribution. When we compare two magnetic measurements at a crossover, from different epochs, the time-varying components of the scalar magnetic equation of measurement are reflected in the residuals.

Nevertheless, in the first part of this study we have considered these differences to be internal in origin. After an analysis of our results, they do not seem to attribute the different *SV* values to the internal origin because they were not only obtained in the same period of time but were also distributed over a small area.

A hypothetical external field origin does not seem plausible either because, as was previously mentioned, both marine cruises were corrected and this time-varying source was extracted.

In our analysis, we have considered the crustal contribution to be invariant in time. When working with magnetic data from a volcanic area, as in our case, this hypothesis is unacceptable. We consider that these different *SV* values are justified by the fact that in the crossover residuals data, obtained throughout the southern area, there was a contribution from the internal origin and also a contribution from a small fraction attributable to a volcano-magnetic signal. If we interpret that a fraction of this residual (-81.1 ± 8.6 nT yr^{-1} vs. -60.8 ± 6 nT yr^{-1}) has a possible volcano-magnetic origin and if we consider that the difference in time between them is 2.2 yr, we may conclude that its amplitude should be 45 nT on average.

Three main mechanisms could account for the observed magnetic variations: (a) thermal magnetisation related to magma cooling below its Curie temperature, (b) piezomagnetic effects and (c) streaming potentials (Zlotnicki & Le Mouel 1988; Del Negro & Ferrucci 2000).

The first mechanism is related to the fact that when magma cools below its Curie temperature it acquires a thermoremanent magnetisation (TRM), conditioned by the intensity and direction of the Earth's magnetic field and by the composition of the magma. TRM is the primary natural remanent magnetisation (NRM) of igneous

Table 4. *SV* solution obtained by using only averages derived from four or more crossovers (see text details).

*SV*1 (nT yr^{-1})	*SV*2 (nT yr^{-1})	*SV*3 (nT yr^{-1})	*SV*4 (nT yr^{-1})	*SV*5 (nT yr^{-1})
−105.6	−98.8	−90.1	−86.5	−83.6

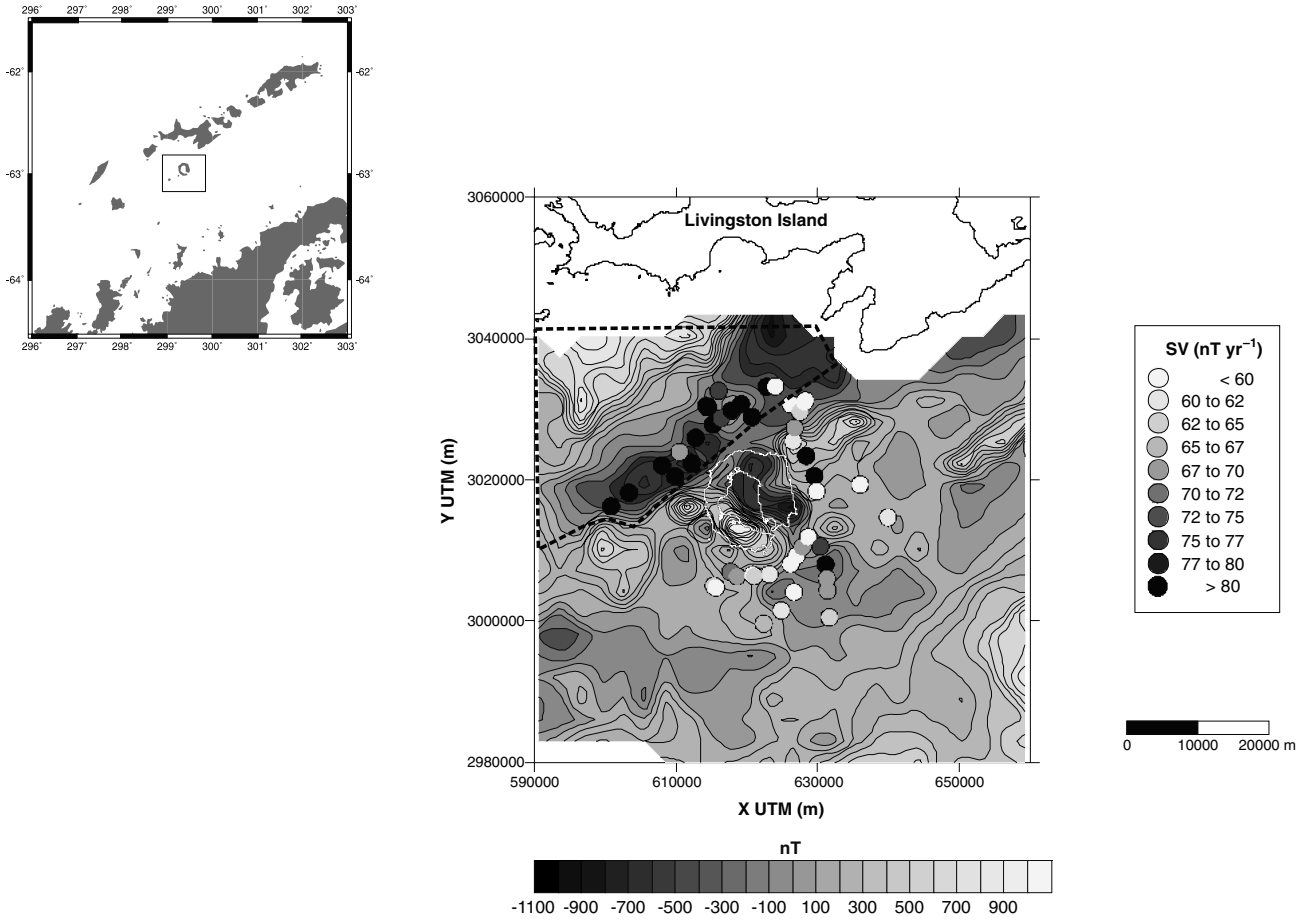

Figure 7. Scalar magnetic map for DI surroundings (modified from Muñoz *et al.* 2005). The *SV* observed for every tie point during the period 1999.9–2002.17 is displayed in grey circle colour code. Contour interval: 100 nT. Note that the *SV* legend shows absolute values.

rocks. The duration of such changes may range from weeks to years, closely conditioned by the size of the body (Del Negro & Ferrucci 1998).

The other two mechanisms, (b) and (c), are related to stress variations. This effect is exclusively reflected, particularly in (b), and its duration is that of the stress field (Zlotnicki & Le Mouel 1988). The last one, (c), is the result of suddenly varying interstitial pressure on the distribution and/or circulation of iron-rich underground waters in a highly fractured rock media (Zlotnicki & Le Mouel 1988; Del Negro & Ferrucci 2000). In relation to thermo-magnetic changes, mechanisms (b) and (c) are faster.

We do not have additional crossovers located elsewhere whose time boundaries forked the 1999–2002 epochs or, alternatively, were near enough for this temporal gap to be sensitive to a 45 nT signal. Therefore, we cannot provide an upper limit for its wavelength. According to our data, Fig. 7 shows that the volcano-magnetic signal apparently has at least a moderate wavelength (it extends at least 30 km around DI).

Moreover, as we only have data from December 1999 and January–February 2002, we do not have a continuous record to infer its timescale. We cannot be sure if this magnetic variation (an average net increase of 45 nT) has taken place in a short period of time or in several events in a step-like fashion or even if it has been extending gradually over this 2-yr period.

This type of irreversible yearly rated change in the magnetic field is difficult to explain by an alteration in rock magnetisation due to mechanical stress (Del Negro & Ferrucci 1998). As the time constants of electrokinetic magnetic fields (streaming potentials) are mainly those of the tectonic (or volcanic) stress field (Zlotnicki & Le Mouel 1988), we could apply the same argument to the latter mechanism.

Considering the reasons given above (the lower bound size of the area where we have detected the change in the magnetic field: at least 30 km), we would suggest that the change in the magnetic field could be attributed to a source with a similar spatial extension. A TRM origin (cooling of a magma intrusion below Curie temperature) could account for this and also for the irreversible increase observed.

The magnetic anomaly map provides a dipolar shape for DI (Muñoz *et al.* 2005, Fig. 5b) which is difficult to appreciate in Fig. 7. Its north-eastern side features negative values with a smoother distribution than its south-western counterpart. This 2-km-wide negative anomaly area extends with a NW–SE trend.

Both areas (south-western side/positive anomalies and north-eastern side/negative values) are separated in the inner bay by a high gradient signal that marks a NW-SE trend and reaches values of 1 nT m^{-1}.

Several authors discuss the long wavelength minimum anomaly that runs through the inner bay with a NW–SE trend. García *et al.* (1990) concluded, by using spectral analysis criteria, that it could be justified by a high-temperature intrusive linear body positioned at a depth of 2 km. Muñoz *et al.* (2005) also interpret this anomaly, by means of forward modelling and Euler Deconvolution techniques, as a partially melted intrusive body with its top estimated to be at a depth of 1.7 km. Considering the wavelength of the *SV* signal (at least 30 km) we shall discuss the possibility that it could be attributed to a progressive cooling of the magma reservoir.

5.2.1 The size of the cooling body

The study of the cooling process from melt temperature to lesser values would serve to model the thermal magnetisation curve as the magma block cools below Curie temperature and is also deeply connected with the size of the causative body. We have checked an approximate solution based on several simplifying assumptions (i.e. disregarding latent heat, assuming that heat is transferred by conduction only). Additionally, we took the thermal diffusivity $\kappa = 0.005$ cm^{-1} s^{-1} which is a good average for this type of magma (Büttner *et al.* 1998; Del Negro & Ferrucci 1998). The resolution of the problem is known as Laplace's solution (Turcotte & Schubert 2002).

Its resolution shows that the temperature T at a certain time t and distance x from the symmetry plane of the magma layer, which is supposed to be perfectly horizontal, is given by (Carslaw & Jaeger 1959):

$$\frac{T}{T_0} = \phi(\xi, \tau) = \frac{1}{2}\left\{\mathrm{erf}\frac{\xi + 1}{2\tau^{\frac{1}{2}}} - \mathrm{erf}\frac{\xi - 1}{2\tau^{\frac{1}{2}}}\right\}, \quad (7)$$

where $\xi = x/a$ and $\tau = \kappa t/a^2$ are two dimensionless parameters, erf is the error function, a is the half-thickness of the magma layer and T_0 its initial temperature.

The intrusion temperature was assumed to be 1100°C, appropriate for basaltic magma.

Eq. (7) was resolved for different values of the half-thickness of the layer (parameter 'a'). We observed that this parameter was critical for the cooling process. The cooling mechanism was only efficient when the half-thickness remained smaller than 5 m; otherwise the temperature remained over $T_{\mathrm{Curie}}(T_c)$ for years.

Therefore, we were able to propose the following reasons for discarding a progressive cooling of the magma reservoir as the source of this possible volcano-magnetic signal: (a) Disregarding latent heat, strictly speaking, would work against the cooling process because it supposes an extra heat input in our process and would reduce the efficiency of the cooling conduction mechanism, increasing the cooling time considerably when the size of the body involved exceeds restrictive size limits.

(b) Nearly 2 yr of progressive cooling of the magma reservoir force us to consider limited thickness for the solidified source (i.e. 5 m). According to Muñoz *et al.* (2005), this layer must be located at a depth of approximately 1.7 km. By forward modelling, we have found that, in order to synthesize a 50 nT-amplitude signal, this block would need a net magnetisation greater than 50 A m^{-1}, which is unacceptable.

In order to enhance the magnetic causative body boundaries, we took advantage of the fact that the 2-D analytical signal produces maxima over magnetic contacts, regardless of the direction of magnetisation or its induced and/or remanent character (Roest *et al.* 1992; Roest & Pilkington 1993).

Fig. 8 shows a wiggle plot where the analytical signal of the DECVOL magnetic profiles are displayed. Filled circles overprint the different crossovers. We may appreciate that there are plenty of points where we have detected an anomalous *SV* (Fig. 8, solid grey circles) which coincides with the presence of analytical signal peaks.

This led us to a more simplistic and realistic model, considering them to be caused by veins or dykes produced by injections of lava into fissures or fractures in the neighbourhood of the magma chamber. This possibility provides us with an additional degree of freedom, namely its closer approach to the surface, and also the possibility that water could improve the efficiency of the cooling mechanism.

5.2.2 The magnetic response of the dyke cooling body

The most abundant magmatic composition in DI extends from basalts to basaltic andesites (Smellie *et al.* 2002). Emeleus (1977) studied seven unoriented rock samples collected from volcanoes on the Raboul caldera (Papua, New Guinea). All samples were basaltic andesites. He showed that the TRM decreases very rapidly over a rather narrow temperature range. Five samples showed a $T_c = 600$°C, and the other two had a $T_c = 400$°C. Samples always show a 50 per cent (or greater) reduction in TRM by 350°C. Concerning their remanent magnetisation (at 100°C), it varies from nearly 20 A m^{-1} to 2 A m^{-1}.

Del Negro & Ferrucci (1998) noted similar general behaviour for basalts in their study. Rocks sampled in different lava flows show high average remanent magnetisation (7.3 A m^{-1}) and acquire 25 per cent remanent magnetisation at $T = 380$°C and 50 per cent at $T = 240$°C, on average, always with $T_c = 500$°C.

Taking into account previous considerations on thermal-demagnetisation curves, we used eq. (7) and tested different possibilities again. We always used the thermal diffusivity $\kappa = 0.005$ cm^2 s^{-2} (Büttner *et al.* 1998; Del Negro & Ferrucci 1998) and the half-thickness $a = 4$ m.

Under these conditions, the intruded magma cools to 390°C after 24 months, which means 25 per cent magnetisation. For the half-thickness $a = 3$ m, the intruded magma cools to 300°C after 24 months, which means nearly 40 per cent magnetisation. Additionally, a full remanent magnetisation (100 per cent) could be obtained in 10 or 15 yr. We saw, once again, that the half-thickness is a critical parameter for cooling below T_c and that we must manage small thickness values.

5.2.3 The 1998–1999 seismic crisis at Deception Island Volcano

Nevertheless, we still need a mechanism or process that, with a yearly or decadal rate scale, could justify the observed intrusions. As has already been noted, DI is an active volcano, with its latest eruptions dated in 1842, 1967, 1969 and 1970. Moreover, during the 1998–1999 austral summer, the pattern of seismic activity at DI suffered a significant change in relation to previous years. This change was characterized by the occurrence of an intense swarm of local earthquakes (two of them of magnitude 2.8 and 3.4). A local seismic network recorded more than 2000 local earthquakes during the period of January–February 1999.

Their hypocentral distribution indicates that the seismicity is clustered at a focal depth of around 2 km, being located mostly within the inner bay of DI. Ibáñez *et al.* (2003) suggest that this seismic

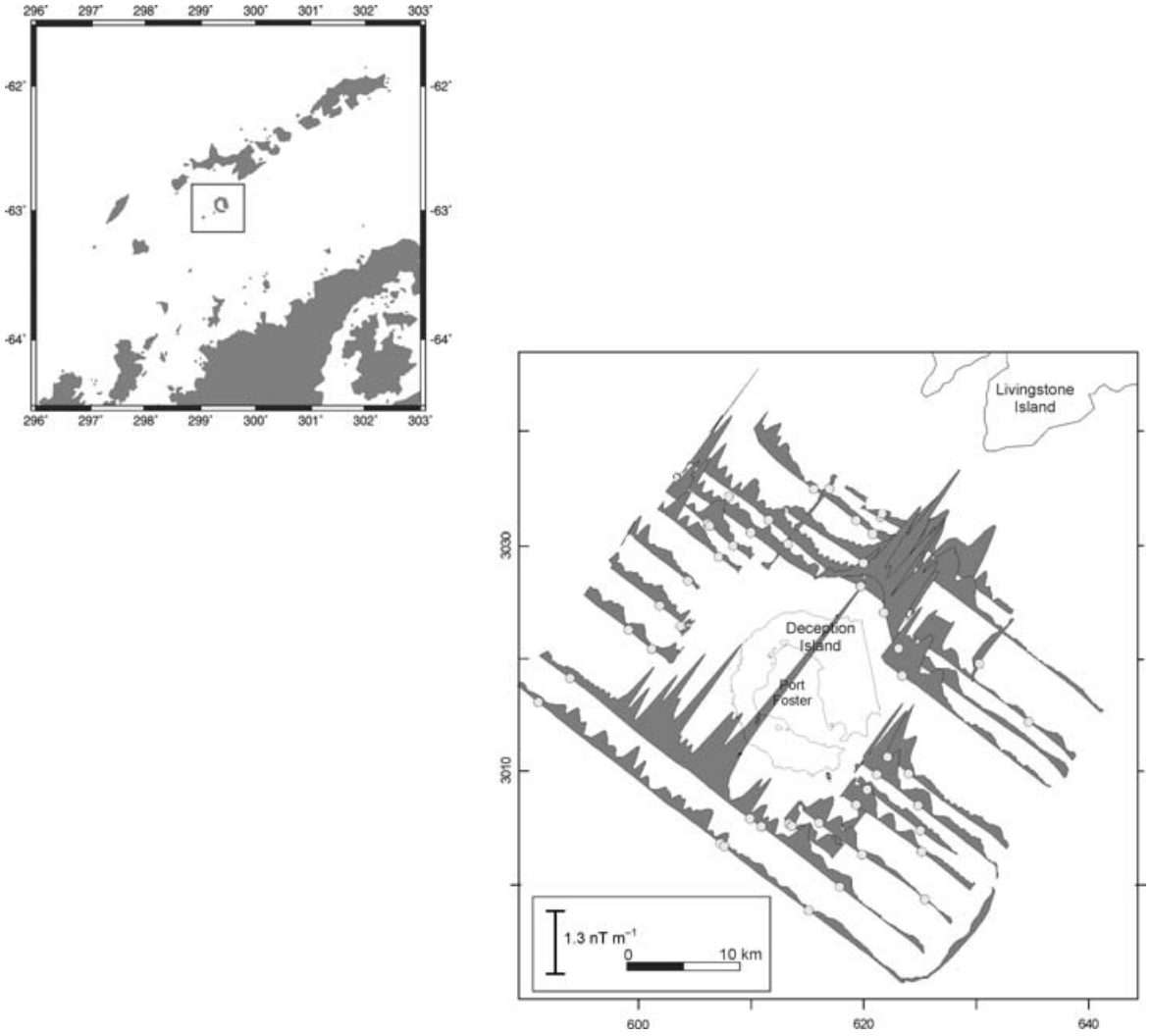

Figure 8. DECVOL's analytical signal profiles displayed as a wiggle plot for DI island surroundings. Grey circles represent tie points.

series was caused by the stress generated by the uplift of the source area due to a magmatic injection in depth.

Such a sequence of events could be related to shallow dyke injections. We could consider the existence of a network of dykes which would have started a slow cooling process and that what we measured in December 1999 and January–February 2002 were isolated values of magnetic readings which show an increase in magnitude according to a thermo-magnetic effect.

We tested a 2.5 magnetic model. In order to narrow down our results we considered a remanent magnetisation of 11 A m^{-1} for the basaltic lava, which is representative of the intensity of magnetisation for dykes at DI (Blanco-Montenegro 1997). The dykes were given 40 per cent magnetisation (i.e. 4.4 A m^{-1}), assuming a Temperature of 300°C after more than 24 months (December 1999 to January 2002). We used local water and sediment layer thicknesses according to Muñoz *et al.* (2005). After trials, the top of the 5-m-wide dyke was set at ≈1000 m. The anomaly vanishes laterally within 0.5 km of its peak.

Our model shows that the range of anomalies observed through the *SV* is compatible with that of a network of dykes that were intruded towards the start of 1999 and slowly froze during the 2 yr that followed.

Taking all these facts into consideration, we suggest that the dichotomy in the *SV* detected between the northern and southern side of DI could be justified by an injection of magma into the local fracture system by means of a process related to the latest volcanic crisis.

6 CONCLUSIONS

By means of magnetic marine data, we have studied the residuals at the different tie points in Bransfield Strait. These residuals contain a variable amount of information related to local geomagnetic *SV*. By applying a simple least-square algorithm we infer different *SV* rates during the 1961–2002 period. Our results have been partially validated by comparing them with local observatory data for the period 1978–2002.

They show the ability to delineate different *SV* horizons which, although simplified, resemble the main features of *SV* variation over

the period of time considered. This idea has been able to detect such yearly changes with a precision limited mainly by the number of samples (only 42) and the external magnetic fields' influence, which acts as noise.

The possibility of using marine magnetic data offers an invaluable source for obtaining historical *SV* values in remote sites where the scientific community lacks this kind of information. Additionally, we believe that with a greater amount of data, regularly as well as conveniently spaced in time, and by performing additional iterative trials, we could include another degree of freedom which would be the jerk occurrence date. This last possibility could help to evaluate the global character of this phenomenon, allowing its analysis to be extended backwards in time.

The second part of this study analyses a special feature, namely the dichotomy in the *SV* series at DI over the 1999–2002 period. We have considered and discussed three possible mechanisms: (a) thermo-magnetic origin, (b) consequences of piezo-magnetic effects and (c) derivation from streaming potentials.

All these sources differ not only in the magnitude of the magnetic anomaly that they are able to produce but also in their time constants. Although we lack information concerning the timescale of this signal, and the way this variation progressed over the 2-yr period (December 1999–February 2002), it is difficult to explain an irreversible yearly rated change by short time effects, such as those that (b) and (c) can justify. We proposed a TRM origin as the most plausible origin for this volcano-magnetic signal.

Its scope, which seems to cover the entire southern part of DI, leads us to a detailed discussion. We have resolved a simplified heat equation which assumes certain approximations (disregarding latent heat, assuming a heat conduction mechanism, etc). We observed that the thickness of the magma layer is critical for the cooling mechanism to be efficient.

We suggest a TRM mechanism, applied on shallow dyke injection intrusions, as the most plausible origin. Forward modelling shows that the amplitude of this magnetic signal (45 nT on average) is compatible with a network of dykes, with a top set at ≈1000 m below sea level, that was intruded towards the start of 1999 as a consequence of a seismic crisis and slowly froze during the 2 yr that followed.

ACKNOWLEDGMENTS

Some figures were drafted with the aid of the Generic Mapping Tools software (Wessel & Smith 1995). We wish to thank Monica Korte and Emma Suriñach who critically read an earlier version of the manuscript and made many helpful suggestions which greatly improved its final version.

REFERENCES

Acosta, J., Herranz, P., Sanz, J.L. & Uchupi, E., 1992. Antarctic continental margin: Geologic image of the Bransfield Trough, an incipient ocean basin, in *Geologic Evolution of Atlantic Continental Rises*, pp. 49–61, eds Poag, C.W. & Graciansky, P.C., Van Nostrand Reinhold, New York.

Alexandrescu, M., Gibert, D., Hulot, G., Le Mouël, J.-L. & Saracco, G., 1996. Worldwide wavelet analysis of geomagnetic jerks, *J. geophys. Res.,* **101,** 21 975–21 994.

Baraldo, A. & Rinaldi, R.A., 2000. Stratigraphy and structure of Deception Island, South Shetland Islands, Antarctica, *J. South American Earth Sci.,* **13,** 785–796.

Barker, D.H.N. & Austin, J.A., 1994. Crustal diapirism in Bransfield Strait, west Antarctica: Evidence for distributed extension in marginal-basin formation, *Geology,* **22,** 657–660.

Barker, D.H.N. & Austin, J.A., 1998. Rift propagation, detachment faulting, and associated magmatism in Bransfield Strait, Antarctic Peninsula, *J. geophys. Res.,* **103,** 24.017–24.043.

Barker, D.H.N., Christeson, G.L., Austin, J.A. & Dalziel, I.W.D., 2003. Backarc basin evolution and cordilleran orogenesis: Insights from new ocean-bottom seismograph refraction profiling in Bransfield Strait, Antarctica, *Geology,* **31**(2), 107–110.

Blanco-Montenegro, I., 1997. Análisis e interpretación de las anomalías magnéticas de tres calderas volcánicas: Decepción (Shetland del Sur, Antártida), Furnas (San Miguel, Azores) y las Cañadas del Teide (Tenerife, Canarias), *PhD thesis*, Universidad Complutense de Madrid.

Bloxham, J., Zatman, S. & Dumberry, M., 2002. The origin of the geomagnetic jerks, *Nature,* **420,** 65–67.

Büttner, R., Zimanowski, B., Blumm, J. & Hagemann, L., 1998. Thermal conductivity of a volcanic rock material (olivine-melilitite) in the temperature range between 288 and 1470 K, *J. Volc. Geotherm. Res.,* **80,** 293–302.

Canals, M. *et al.*, 1994. La Cuenca Central de Bransfield (NW de la Península Antártica): Primeros resultados de la Campaña Gebra 93, *Geogaceta,* **16,** 132–135.

Carslaw, H.S. & Jaeger, J.C., 1959. *Conduction of Heat in Solids*, 2nd edn, Oxford University Press, Oxford.

Del Negro, C. & Ferrucci, F., 1998. Magnetic history of a dyke on Mount Etna (Sicily), *Geophys. J. Int.,* **133,** 451–458.

Del Negro, C. & Ferrucci, F., 2000. Volcanomagnetic effects at Vulcano Island (Aeolian archipelago, Italy), *Geophys. J. Int.,* **140,** 83–94.

De Michelis, P., Cafarella, L. & Meloni A., 1998. Worldwide character of the 1991 geomagnetic jerk, *Geophys. Res. Lett.,* **25,** 377–380.

De Michelis, P., Cafarella, L. & Meloni, A., 2000. A global analysis of the 1991 geomagnetic jerk, *Geophys. J. Int.,* **143,** 545–556.

Emeleus T.G., 1977. Thermo-Magnetic measurements as a possible tool in the prediction of volcanic activity in the volcanoes of the Rabaul Caldera, Papua New Guinea, *J. Volc. Geotherm. Res.,* **2,** 343–359.

García, A., Viramonte, J.G., Via, J. & Ibáñez, J.M., 1990. Estudio del campo magnético en Port Foster (Isla Decepción), in *Actas del III symposium español de estudios antárticos*, pp. 244–249, ed. Castellví, J., C.I.C.Y.T., Madrid.

Garrett, S.W., 1990. Interpretation of reconnaissance gravity and aeromagnetic surveys of the Antarctic Peninsula, *J. geophys. Res.,* **95,** 6759–6777.

González-Ferrán, O., 1991. The Bransfield Rift and its active volcanism, in *Geological Evolution of Antarctica*, pp. 505–509, eds Thomson, R.A., Crame, J.A. & Thomson, J.W., Cambridge University Press, Cambridge.

González-Casado, J.M., López-Martínez, J. & Durán, J.J., 1999. Active tectonics and morphostructure at the northern margin of central Bransfield Basin, Hurd Peninsula, Livingston Island (South Shetland Islands), *Antarctica Sci.,* **11**(3), 323–311.

González-Casado, J.M., Giner-Robles, J. & López-Martínez, J., 2000. Bransfield Basin, Antarctic Peninsula: Not a normal backarc basin, *Geology,* **28,** 1043–1046.

Gràcia, E., Canals, M., Farràn, M., Prieto, M.J., Sorribas, J. & Gebra Team, 1996. Morphostructure and evolution of the Central and Eastern Bransfield Basins (NW Antarctic), *Mar. geophys. Res.,* **18**(1–3), 429–448.

Gràcia, E., Canals, M., Farràn, M., Sorribas, J. & Pallás, R., 1997. The Central and Eastern Bransfield basins (Antarctica) from high-resolution swath-bathymetry data, *Antarctica Sci.,* **9**(2), 168–180.

Grad, M., Guterch, A. & Sroda, P., 1992. Upper Crustal Structure of Deception Island area, Bransfield Strait, West Antarctica, *Antarctica Sci.,* **4**(4), 469–476.

Ibáñez, J.M., Del Pezzo, E., Almendros, J., LaRocca, M., Alguacil, G., Ortiz, R. & García, A., 2000. Seismovolcanic signals at Deception Island volcano, Antarctica: Wave field analysis and source modeling, *J. geophys. Res.,* **105,** 13 905–13 931.

Ibáñez, J.M., Carmona, E., Almendros, J., Saccorotti, G., del Pezzo, E., Abril, M. & Ortiz, R., 2003. The 1998–1999 seismic crisis at Deception Island Volcano, Antarctica, *J. Volc. Geotherm. Res.,* **128,** 65–88.

International Association of Geomagnetism and Aeronomy (IAGA), Division V, Studying Group 8, 2003. The 9th-Generation International Geomagnetic Reference Field, *Geophys. J. Int.,* **155,** 1051–1056.

Lawver, L.A., Sloan, B.J., Barker, D.H.N., Ghidella, M., Von Herzen, R.P., Keller, R.A., Klinkhammer, G.P. & Chin, C.S., 1996. Distributed, active extension in Bransfield Basin, Antarctic Peninsula: Evidence from Multibeam Bathymetry, *GSA Today,* **6**(11), 1–6.

Mandea, M., Bellanger, E. & Le Mouël J.-L., 2000. A geomagnetic jerk for the end of the 20th century?, *Earth planet. Sci. Lett.,* **183,** 369–373.

Metzger, D. & Campagnoli, J., 2003. Marine Trackline Geophysics Data on DVD, Version 4.1.18, National Geophysical Data Center.

Muñoz, A., Catalán, M., Martín, J. & Carbó, A., 2005. Upper crustal structure of Deception Island area (Bransfield Strait, Antarctica) from gravity and magnetic modelling, *Antarctica Sci.,* **17**(2), 213–224.

Paige, C. & Saunders, M., 1982. LSQR: An Algorithm for Sparse Linear Equations and Sparse Least Squares, *ACM Transactions on Mathematical Software,* **8,** 43–71.

Parra, J.C., Gonzalez-Ferrán, O. & Bannister, J., 1984. Aeromagnetic Survey over the South Shetland Islands, Bransfield Strait and part of the Antarctic Peninsula, *Revista Geológica de Chile,* **23,** 3–20.

Pelayo, A.M. & Wiens, D.A., 1989. Seismotectonics and relative plate motions in the Scotia Sea Region, *J. geophys. Res.,* **94,** 7293–7320.

Polish Academy of Sciences, 1998. Results of geomagnetic observations, Arctowski Antarctic station, 1994–1995, C-63 (300), pp. 90, Institute of Geophysics, Warszawa.

Prieto, M.J., Canals, M., Ercilla, G. & Batist, M., 1998. Structure and geodynamic evolution of the Central Bransfield Basin (NW Antarctica) from seismic reflection data, *Mar. Geol.,* **149,** 17–38.

Roach, P.J., 1978. The nature of back-arc extension in Bransfield Strait, *Geophys., J.R. astr. Soc.,* **53,** 165.

Roest, W.R. & Pilkington, M., 1993, Identifying remanent magnetisation effects in magnetic data, *Geophysics,* **58,** 653–659.

Roest, W.R., Verhoef, J. & Pilkington, M., 1992, Magnetic interpretation using the 3-D analytic signal, *Geophysics,* **57,** 116–125.

Smellie, J.L., López-Martinez, J. & others, 2002. Geology and geomorphology of Deception Island, 78 pp., with accompanying maps, BAS GEOMAP Series, Sheets 6-A and 6-B, 1:25000, eds López-Martinez, J., Smellie J.L., Thomson, J.W. & Thomson, M.R.A., British Antarctic Survey, Cambridge.

Thakur, N.K., Gangadhara Rao, T., Subrahmanyam, C. & Khanna, R., 1999. Crossover analysis of geophysical data in Bay of Bengal, *Geo-Marine Letters,* **19,** 262–269.

Torta, J.M., Gaya-Piqué, L.R., Solé, J.G., Blanco, I. & García A., 1999. A new geomagnetic observatory at Livingston Island (South Shetland Islands): Implications for future regional magnetic surveys, *Annali di Geofisica,* **42,** 141–151.

Torta, J.M., Gaya-Piqué, L.R., Riddick, J.C. & Turbitt, C.W., 2001. A partly manned geomagnetic observatory in Antarctica provides a reliable data set, *Contribution to Geophysics and Geodesy,* **31/1,** 225–230.

Turcotte, D.L. & Schubert, G., 2002. *Geodynamics*, 2nd edn, 456 pp., Cambridge University Press, United Kingdom.

Wessel, P. & Smith, W.H.F., 1995, New version of the Generic Mapping Tools released, *EOS, Trans. Am. geophys. Un.,* **76,** 329.

Wessel, P. & Watts, A.B., 1988. On the accuracy of marine gravity measurements, *J. geophys. Res.,* **93,** 393–413.

Zlotnicki, J. & Le Mouel, J.-L., 1988. Volcanomagnetic effects observed on Piton de la Fournaise volcano (Reunion Island): 1985–87, *J. geophys. Res.,* **93,** 9157–9171.